Supporting Information

Polymorphism, ionic conductivity and electrochemical properties of lithium *closo*-deca- and dodeca borates and composites, $Li_2B_{10}H_{10}$ - $Li_2B_{12}H_{12}$

Chongyang Zhou[a,b], Jakob B. Grinderslev[a], Lasse N. Skov[a], Mathias Jørgensen[a], Yuanzhi Li[b], Jørgen Skibsted[a], Yigang Yan[c]* and Torben R. Jensen[a]*

[a] *Interdisciplinary Nanoscience Center (iNANO) and Department of Chemistry, Aarhus University, Langelandsgade 140, 8000 Aarhus C, Denmark. E-mail: trj@chem.au.dk*

[b] *State Key Laboratory of Silicate Materials for Architectures (Wuhan University of Technology), 122 Luoshi Road, Wuhan 430070, P. R. China.*

[c] *Institute of New Energy and Low-Carbon Technology, Sichuan University, Chengdu 610207, China. E-mail: yigang.yan@scu.edu.cn*

Corresponding author: Torben R. Jensen (trj@chem.au.dk)

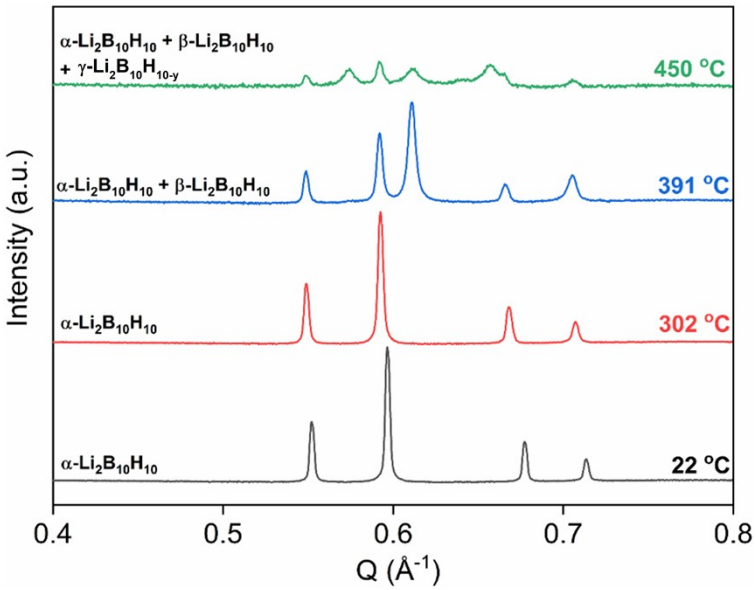

Figure S1. Selected SR PXD patterns of $Li_2B_{10}H_{10}$ (**s1**) obtained from the *in-situ* SR PXD experiment (λ = 0.826927 Å, $\Delta T/\Delta t$ = 5 °C/min, p(Ar) = 1 bar).

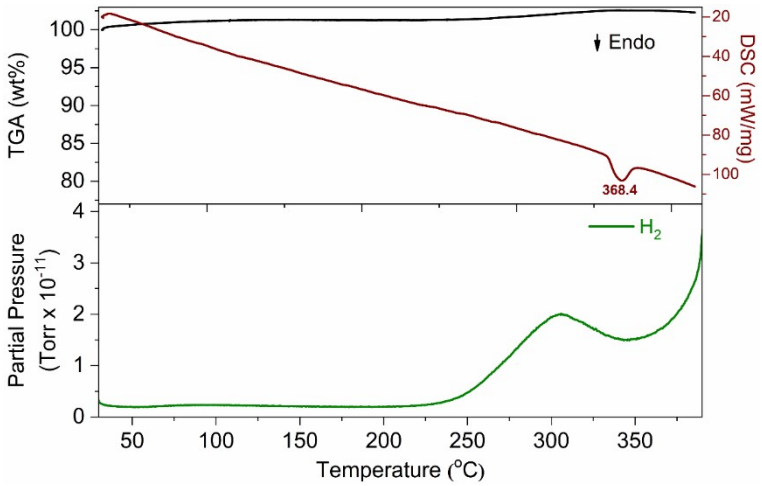

Figure S2. Anhydrous α-$Li_2B_{10}H_{10}$ (**s1**) investigated by simultaneous thermogravimetric analysis (TGA), differential scanning calorimetry (DSC) and mass spectrometry (MS). Sample **s1** is heated from 30 to 390 °C ($\Delta T/\Delta t$ = 5 °C/min, argon flow 30 mL/min).

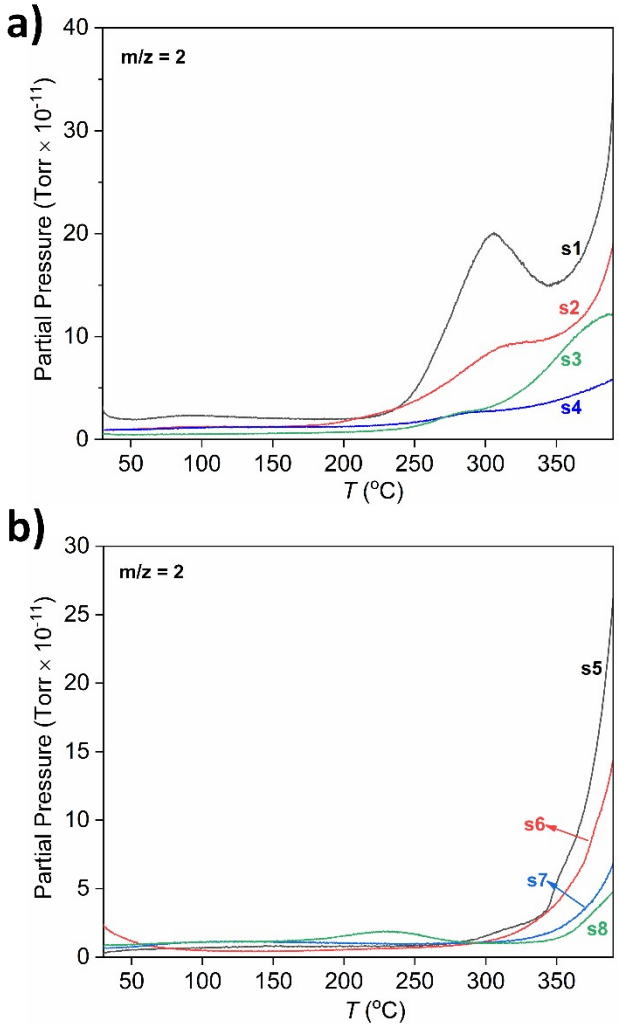

Figure S3. Mass spectrometry (*m*/*z* = 2) profiles for **a)** samples **s1** to **s4**, **b)** samples **s5** to **s8**.

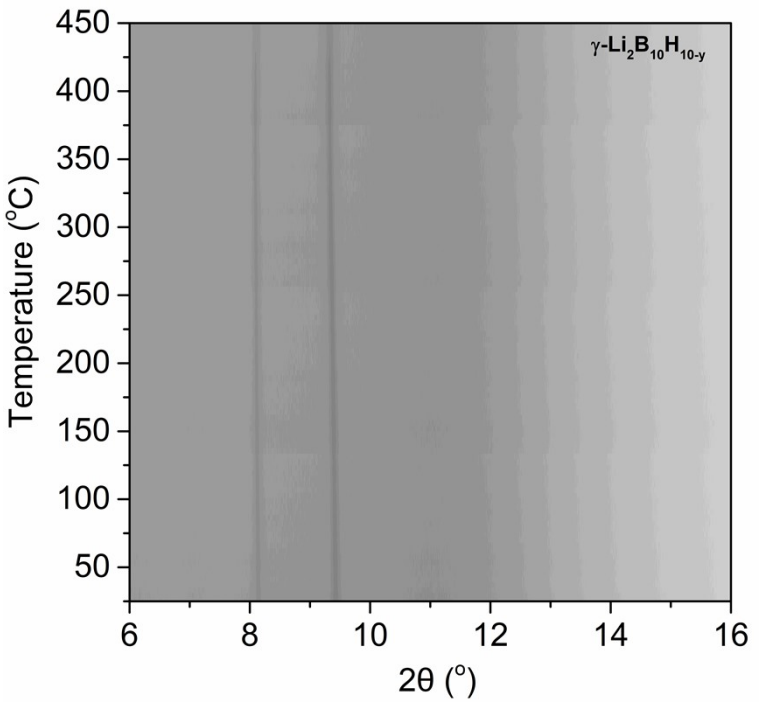

Figure S4. *In situ* SR PXD data for $Li_2B_{10}H_{10}$ heated in H_2 (**s4**) (λ = 0.826927 Å, $\Delta T/\Delta t$ = 5 °C min^{-1}, p(Ar) = 1 bar).

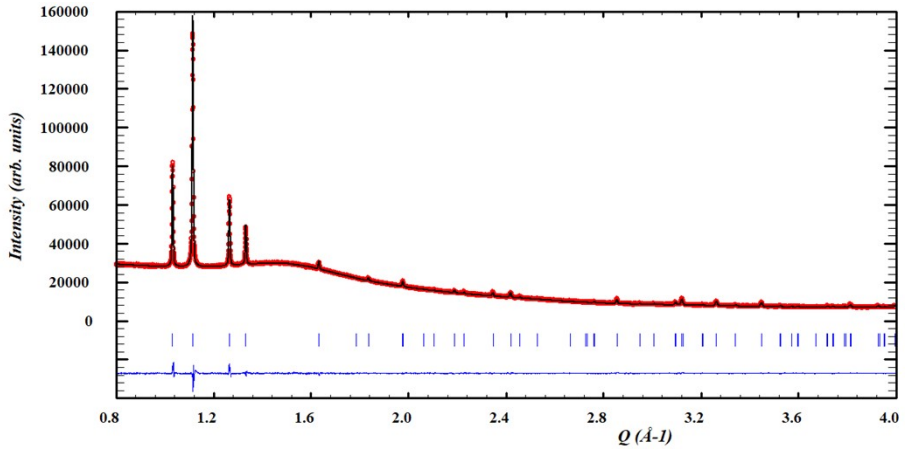

Figure S5. Rietveld refinement of 'as-prepared' α-$Li_2B_{10}H_{10}$ (**s1**) from SR PXD data measured at T = 22 °C, λ = 0.826927 Å, showing experimental (red circles) and calculated (black line) PXD patterns, and a difference plot below (blue line). Blue tick marks: α-$Li_2B_{10}H_{10}$. Final discrepancy factors: R_p = 0.847 %, R_{wp} = 1.28 % (not corrected for background), R_p = 20.2 %, R_{wp} = 9.64 % (conventional Rietveld R-factors), R_{Bragg}(α-$Li_2B_{10}H_{10}$) = 4.29 % and global χ^2 = 2.24.

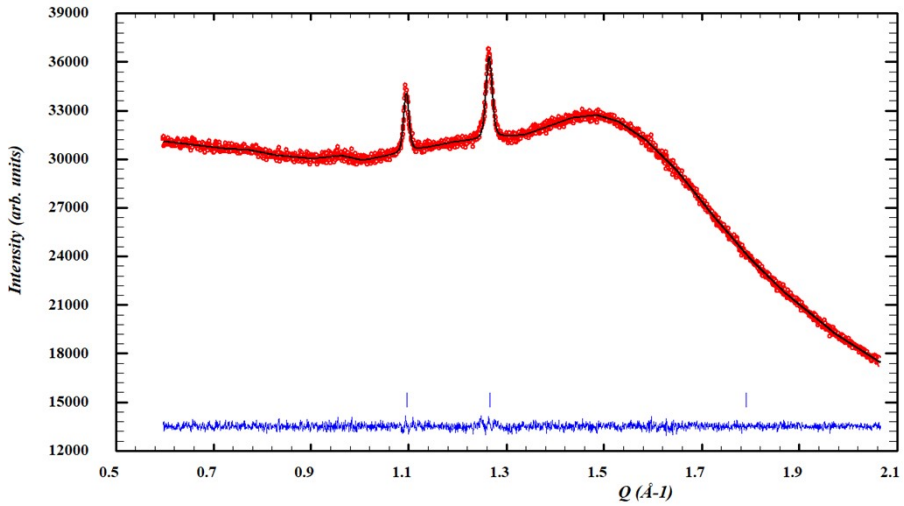

Figure S6. Rietveld refinement of SR PXD data measured at T = 22 °C of $Li_2B_{10}H_{10}$ heated at 380 °C in $p(H_2)$ = 450 bar (**s4**) from, λ = 0.826927 Å, showing experimental (red circles) and calculated (black line) PXD patterns, and a difference plot below (blue line). Blue tick marks: Le Bail fit of γ-$Li_2B_{10}H_{10-y}$. Final discrepancy factors: R_p = 0.441 %, R_{wp} = 0.561 % (not corrected for background), R_p = 95.2 %, R_{wp} = 27.6 % (conventional Rietveld R-factors), R_{Bragg}(γ-$Li_2B_{10}H_{10-x}$) = 0.0428 % and global χ^2 = 1.08.

Table S1. Structural parameters of β-$Li_2B_{10}H_{10}$ (**s1**) at T = 391 °C: Space group Fm-3m, a = 9.567(1) Å, V = 875.7(2) Å^3.

Atom	*x/a*	*y/b*	*z/c*	Occupancy
Li[(a)]	0.25	0.25	0.25	1
B1	0.806	0	0	1/3
B2	0.936	0.8763	0.936	1/3
H1	0.6903	0	0	1/3
H2	0.8968	0.775	0.8968	1/3

[(a)] The atomic positions of Li is a suggested average position based on the structural resemblance to *ht*-$Na_2B_{10}H_{10}$ and β-$Ag_2B_{10}H_{10}$.

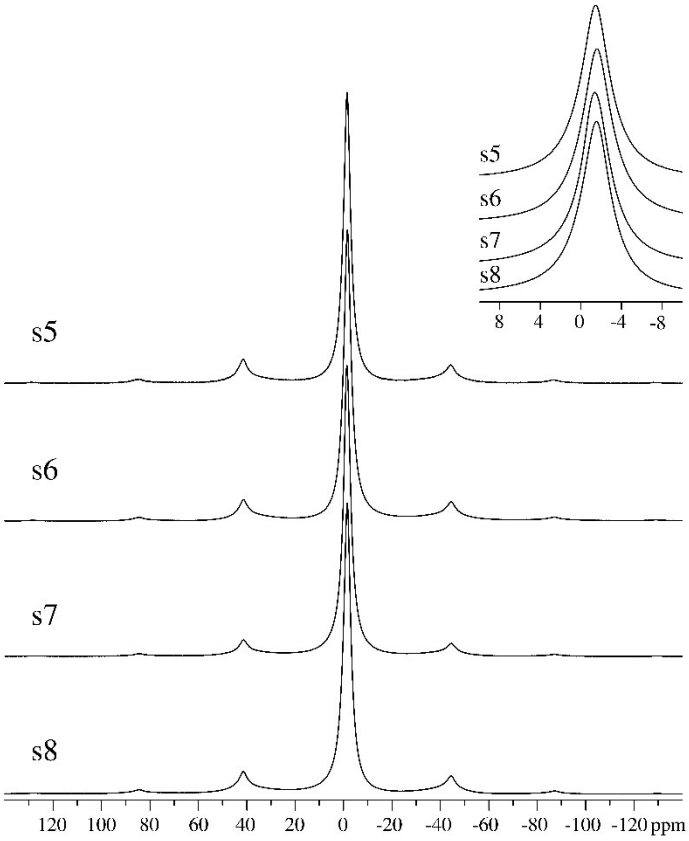

Figure S7. ^{7}Li MAS NMR spectra of the $Li_2B_{12}H_{12}$ samples **s5** to **s8**, obtained at 14.09 T using a spinning speed of ν_R = 12.0 kHz.

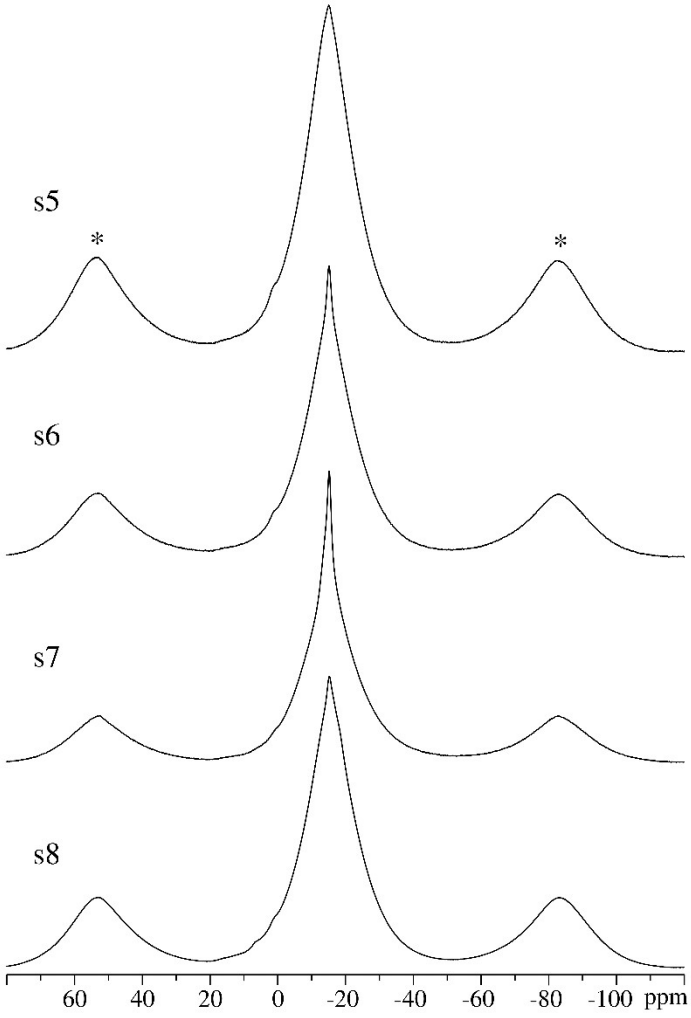

Figure S8. ^{11}B MAS NMR spectra (14.09 T, ν_R = 13.0 kHz), illustrating the central transition region for the $Li_2B_{12}H_{12}$ samples **s5** to **s8**. Spinning sidebands are marked by asterisks in the upper spectrum.

Table S2. Lattice parameters of $Li_2B_{12}H_{12}$ extracted from Rietveld refinements of samples **s5** and **s9** to **s16**.

Sample	Lattice param. *a* (Å)
s5	9.568(3)
s9	9.570(2)
s10	9.570(5)
s11	9.570(9)
s12	9.569(1)
s13	9.571(8)
s14	9.576(2)
s15	9.569(5)
s16	9.571(4)

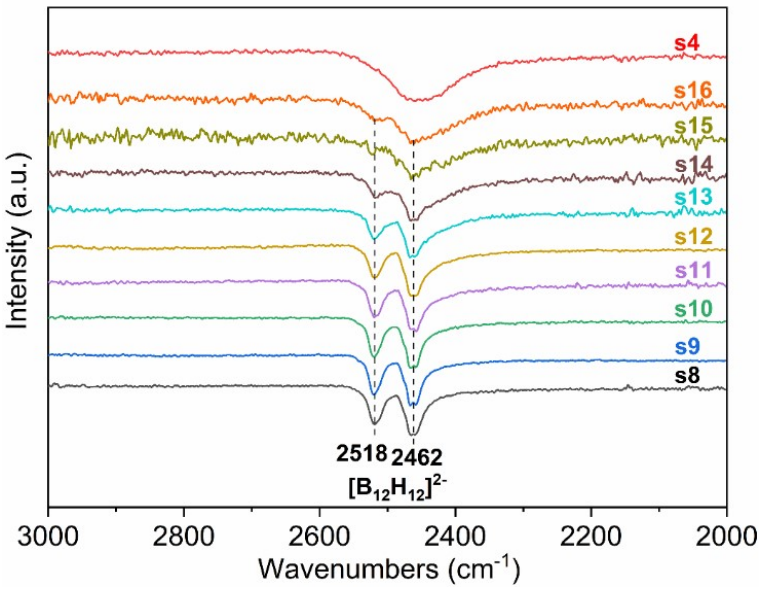

Figure S9. Fourier-transform infrared spectroscopy (FTIR) of $Li_2B_{10}H_{10}$ - $Li_2B_{12}H_{12}$ composite samples **s9** to **s16** compared to $Li_2B_{10}H_{10}$ (**s4**) and $Li_2B_{12}H_{12}$ (**s8**) thermally treated in the same manner (T = 380 °C and $p(H_2)$ = 450 bar). All FTIR data are measured at room temperature.

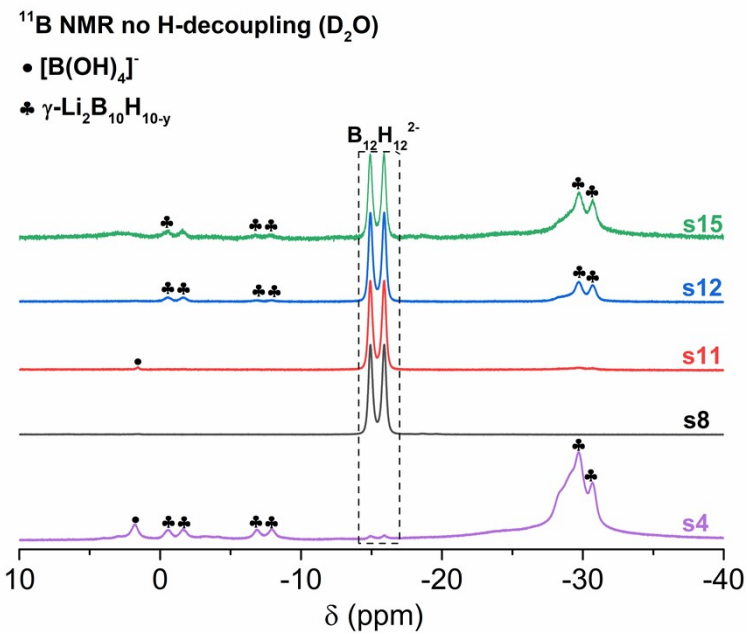

Figure S10. Liquid phase ^{11}B NMR spectroscopy without proton decoupling of samples **s4**, **s8**, **s11**, **s12** and **s15**.

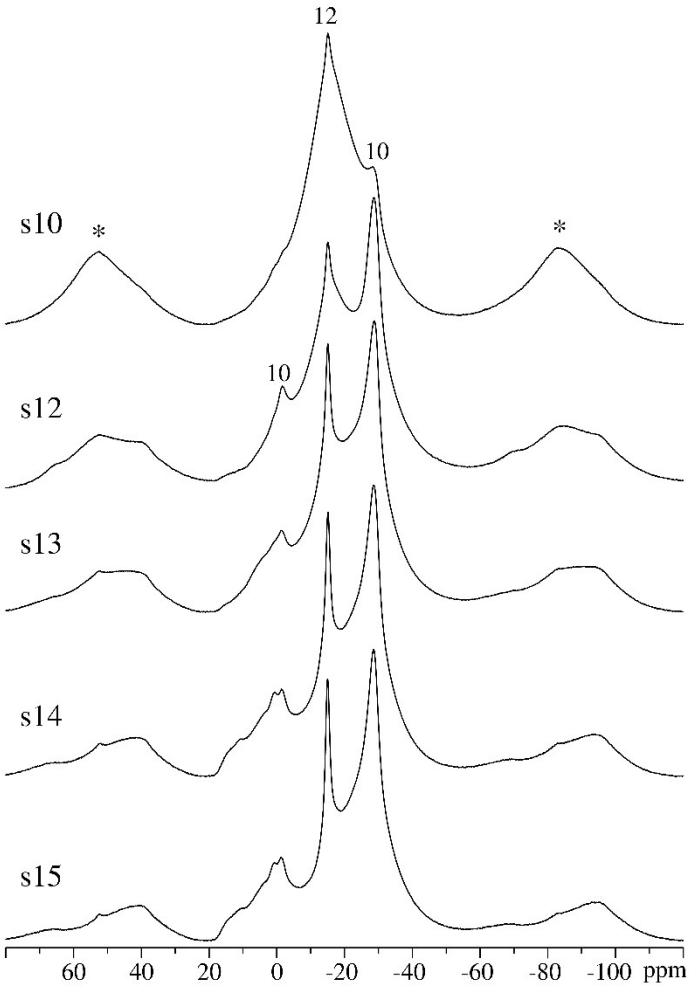

Figure S11. ^{11}B MAS NMR spectra (14.09 T, ν_R = 13.0 kHz), illustrating the central transition region for the composite (1-*x*)$Li_2B_{12}H_{12}$–*x*$Li_2B_{10}H_{10}$ samples **s10** and **s12** to **s15**. Spinning sidebands are marked by asterisks in the upper spectrum. The principal centerband resonances from the $Li_2B_{10}H_{10}$ and $Li_2B_{12}H_{12}$ phases are marked by 10 and 12, respectively.

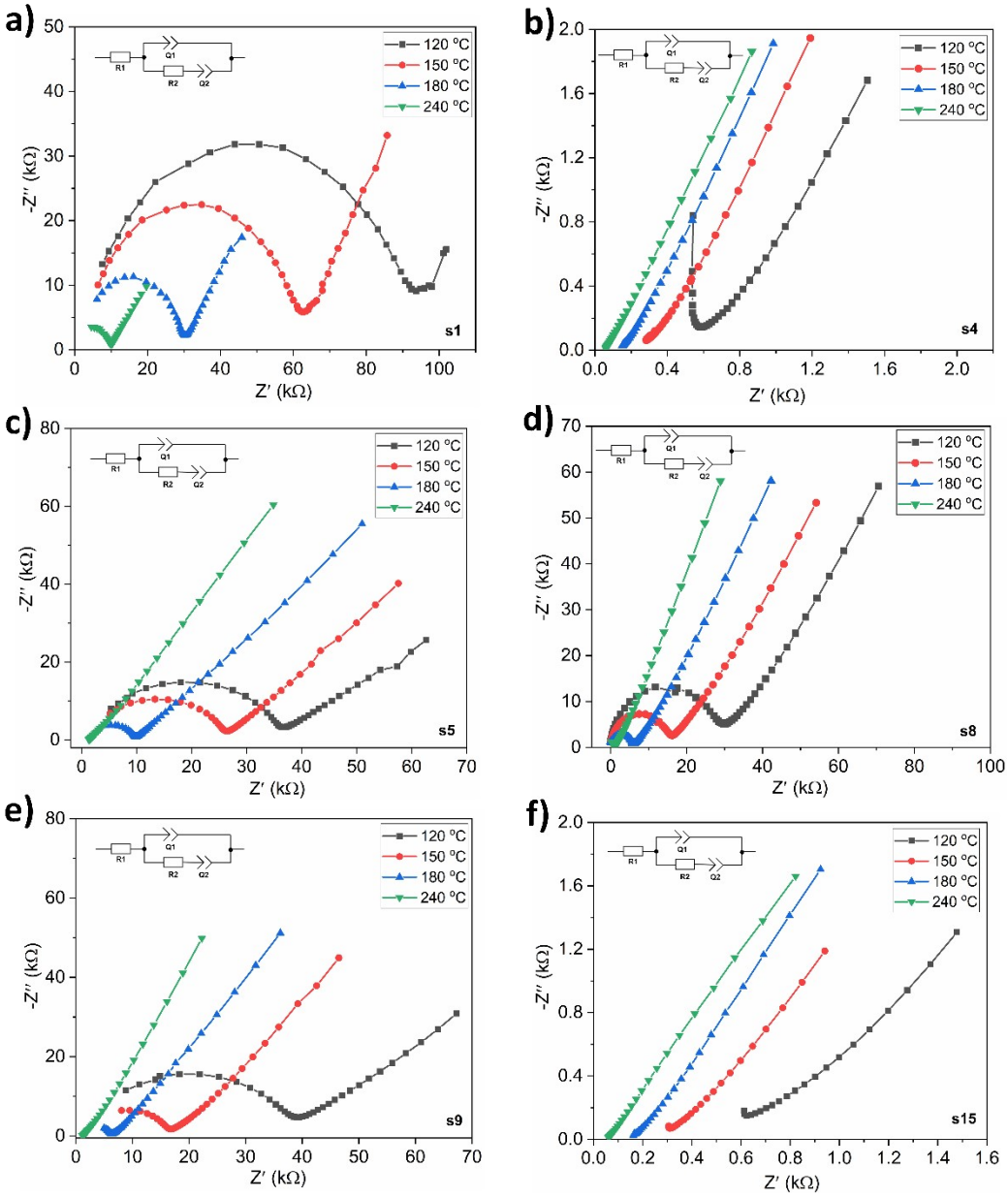

Figure S12. Selected Nyquist plots of impedance data of samples **a) s1**, **b) s4**, **c) s5**, **d) s8**, **e) s9** and **f) s15**. These examples indicate impedance curves recorded for samples at different temperatures during heating of the sample.

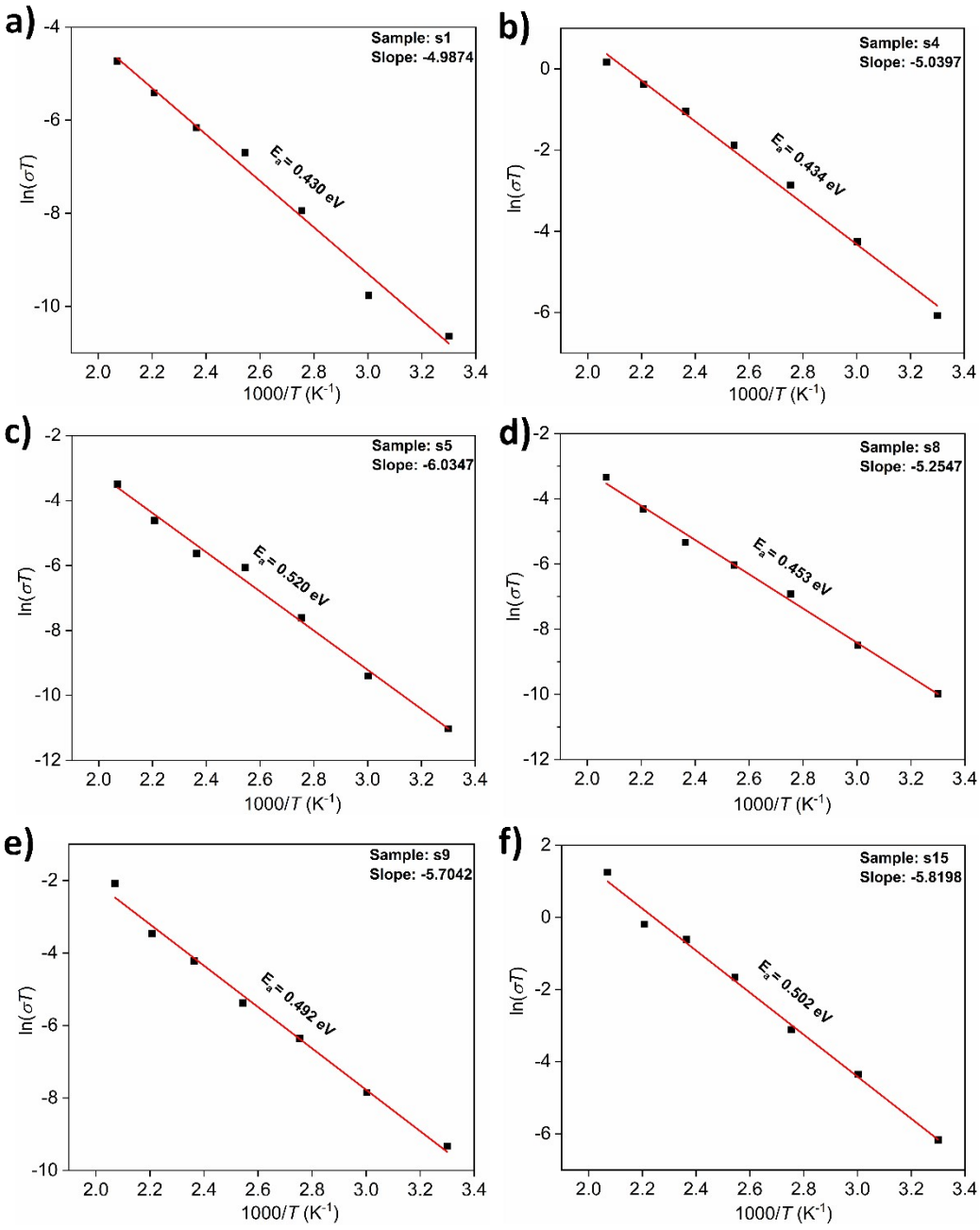

Figure S13. The activation energies, E_a of samples **a) s1**, **b) s4**, **c) s5**, **d) s8**, **e) s9** and **f) s15**. The temperature ranges from 30 to 210 °C during the heating process.

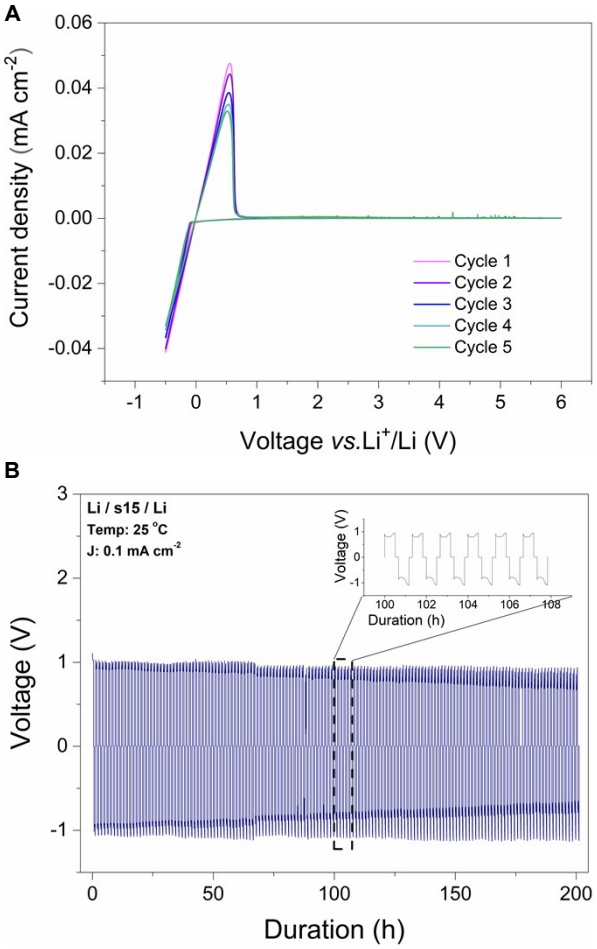

Figure S14. A) Cyclic voltammogram curves of Li|SSE|SS in the potential range -0.5 to 6 V vs. Li/Li^+ (SSE: **s15**, SS: stainless steel). **B)** Galvanostatic cycling of a symmetric Li|SSE|Li cell at 25 °C with a constant current density of 0.1 mA cm^{-2} (SSE: **s15**). The inset shows a zoom-in of the voltage profile during the cycling. A small polarization is observed during the measurement, which indicate a too low cell pressure to maintain interfacial contact during cycling.